Journal of Applied Mechanics and Technical Physics, Vol. 35, No. 2, 1994

INTERACTION OF A SHOCK WAVE WITH A CLOUD OF PARTICLES OF FINITE DIMENSIONS

V. P. Kiselev, S. P. Kiselev, and V. M. Fomin

UDC 532.539

This article presents results of calculations of the interaction of a shock wave (SW) with a cloud of particles. It is shown that the volume concentration of particles has a substantial effect on the acceleration of the cloud.

1. We will examine a cloud of solid spherical particles in the path of a shock wave. It is necessary to find the parameters of the gas and particles that result from the interaction of the wave with the cloud. The motion of the particles is modeled by a non-collisional kinetic equation, while the motion of the gas is modeled by the averaged equations of a dust-bearing gas. It is assumed that the particles may be dispersed with respect to velocity and size. The given model was described in detail in [1, 2] and can be used in the case when either the particle trajectories do not intersect within the flow region or particle collisions are rare ($\mathrm{Kn} \approx d/(6m_2L) \gtrsim 1$, L being the relative distance travelled by a particle in the cloud, m_2 the volume concentration of particles, and d particle diameter). Ignoring the effects of heat transfer, we write the complete system of equations [1, 2] in the form

$$\frac{\partial f}{\partial t} + \nabla_i v_2^i f + \frac{\partial}{\partial v_2^i}(a^i f) = 0, \quad i = 1,2,3,$$

$$f = f(t,x^i,v_2^i,r_s), \quad n = \int_{-\infty}^{\infty}\int_{0}^{\infty} f dV_v dr_s,$$

$$m_2 = \int_{-\infty}^{\infty}\int_{0}^{\infty} \frac{4}{3}\pi r_s^3 f dV_v dr_s, \quad dV_v = dv_2^1 dv_2^2 dv_2^3,$$

$$m_1 + m_2 = 1, \quad \rho_2 = \rho_{22} m_2, \quad a^i = a_v^i - \nabla_i p/\rho_{22},$$

$$a_v^i = \frac{3}{4}\left(\frac{\mathrm{Re}\,\mu}{\rho_{22} d^2}\right) C_d(\mathrm{Re},\mathrm{M}_{12})(v_1^i - v_2^i),$$

$$C_d(\mathrm{Re},\mathrm{M}_{12}) = (1 + \exp(-0.43/\mathrm{M}_{12}^{4.67}))\left(\zeta + \frac{24}{\mathrm{Re}} + \frac{4}{\sqrt{\mathrm{Re}}}\right),$$

$$\mathrm{Re} = \rho_{11}|v_1 - v_2| d/\mu, \quad \mathrm{M}_{12} = |v_1 - v_2|/c_0, \tag{1.1}$$

$$p = (\gamma - 1)\rho_{11}\mathscr{E}_1, \quad \mathscr{E}_1 = c_V T_1, \quad \rho_1 = \rho_{11} m_1, \quad \frac{\partial \rho_1}{\partial t} + \nabla_i(\rho_1 v_1^i) = 0,$$

$$\rho_1 \frac{d_1 v_1^i}{dt} = -m_1 \nabla_i p - F_{12}^i, \quad \frac{d_1}{dt} = \frac{\partial}{\partial t} + v_1^i \nabla_i,$$

$$\frac{d_1 \mathscr{E}_1}{dt} + p\frac{d_1}{dt}\left(\frac{1}{\rho_{11}}\right) = \Phi_3, \quad F_{12}^i = \int_{-\infty}^{\infty}\int_{0}^{\infty} m a_v^i f dV_v dr_s, \quad m = \frac{4}{3}\pi r_s^3 \rho_{22},$$

$$\Phi_3 = \frac{1}{\rho_1}\int_{-\infty}^{\infty}\int_{0}^{\infty} m a_v^i (v_1^i - v_2^i) f dV_v dr_s,$$

where summation is performed over repeating indices i; f is the one-particle distribution function in the phase space t, x^i, v_2^i, r_s (i = 1, 2, 3); dV_v is an element of volume in the velocity space; n is concentration; a^i, $\langle v_2^i \rangle$ are the i-th components of particle acceleration and mean velocity; p, μ, and c_0 are pressure, viscosity, and sonic velocity in the gas; γ is the adiabatic exponent; Re and M_{12} are the Reynolds and Mach numbers; m_1, m_2, ρ_1, ρ_2, ρ_{11}, ρ_{22} are the volume concentrations, mean densities, and true densities of the gas and particles; $\mathscr{E}_1$ is the specific energy of the gas; F_{12}^i the i-th component of the force of gas-particle interaction, associated with velocity disequilibrium. Here, we calculate the motion of the gas and particles in

Novosibirsk. Translated from Prikladnaya Mekhanika i Tekhnicheskaya Fizika, No. 2, pp. 26-37, March-April, 1994. Original article submitted April 13, 1993.

0023-8944/94/3502-0183$12.50

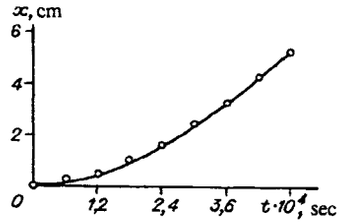

Fig. 1

the axisymmetric and plane cases. Since the cloud may move large distance when accelerating, it is best to solve the problem in a system based on the center of mass of the cloud. Directing the z axis along the velocity of the center of mass D and directing r perpendicular to this velocity, we rewrite system (1.1) as follows:

$$\frac{\partial f}{\partial t} + v_2\frac{\partial f}{\partial z} + w_2\frac{\partial f}{\partial r} + \frac{\partial}{\partial v_2}(a_z f) + \frac{\partial}{\partial w_2}(a_r f) + k\frac{w_2}{r}f = 0,$$

$$v_2 = v_2^l - D,\ w_2 = w_2^l,\ a_z = a_z^l - \dot{D},\ a_r = a_r^n,$$

$$\dot{D} = \frac{dD}{dt},\ D = \int \rho_2 v_2^l f dV dV_v dr_s / \int \rho_2 f dV dV_v dr_s,$$

$$dV = r^k dr dz,\ dV_v = dw_2 dv_2,\ \frac{\partial \varphi}{\partial t} + \frac{\partial F}{\partial z} + \frac{\partial G}{\partial r} + \Phi = 0,$$

$$\varphi = \begin{pmatrix} \rho_1 \\ \rho_1 v_1 \\ \rho_1 w_1 \\ \rho_1\left(\mathscr{E}_1 + \dfrac{v_1^2 + w_1^2}{2}\right) \end{pmatrix},\quad F = \begin{pmatrix} \rho_1 v_1 \\ \rho_1 v_1^2 + pm_1 \\ \rho_1 v_1 w_1 \\ \rho_1 v_1 A_1 \end{pmatrix},$$

$$G = \begin{pmatrix} \rho_1 w_1 \\ \rho_1 v_1 w_1 \\ \rho_1 w_1^2 + pm_1 \\ \rho_1 w_1 A_1 \end{pmatrix},\quad \Phi = \begin{pmatrix} k\rho_1 w_1/r \\ k\rho_1 v_1 w_1/r + \Phi_1 \\ k\rho_1 w_1^2/r + \Phi_2 \\ k\rho_1 w_1 A_1 + A_2 \end{pmatrix}, \qquad (1.2)$$

$$v_1 = v_1^l - D,\ w_1 = w_1^l,\ A_1 = \mathscr{E}_1 + pm_1/\rho_1 + (v_1^2 + w_1^2)/2,$$

$$A_2 = v_1\Phi_1 + w_1\Phi_2 + p\left(\frac{\partial m_1}{\partial t} + v_1\frac{\partial m_1}{\partial z} + w_1\frac{\partial m_1}{\partial r}\right) - \rho_1\Phi_3,$$

$$\Phi_1 = \rho_1\dot{D} - p\frac{\partial m_1}{\partial z} - F_{12}^z,\ \Phi_2 = -p\frac{\partial m_1}{\partial r} - F_{12}^r,$$

$$\Phi_3 = \frac{1}{\rho_1}\int m(a_v^z(v_1 - v_2) + a_v^r(w_1 - w_2))fdV_v dr_s.$$

Here, k = 0 in the plane case and k = 1 in the axisymmetric case; v_1, v_2, w_1, and w_2 are the z- and r-components of the velocities of the gas and particles; an *l* superscript denotes the parameters of the gas and particles in the laboratory coordinate system. The remaining notation is the same as in Eqs. (1.1).

System (1.1)-(1.2) is used to calculate the subsonic ($M_{12} < 1$) and supersonic ($M_{12} > 1$) motions of the particles in the gas. In the case of supersonic motion, a conical Mach wave forms near each particle. This model does not permit calculation of the shock wave "sitting" on a given particle, but the presence of the wave is accounted for in the relation $C_d(M_{12})$. Thus, $C_d(M_{12} > 1)/C_d(M_{12} < 1) \sim 2$. This makes it possible to correctly describe the averaged supersonic motion of the cloud in the gas. The coefficient ζ in the formula for C_d (see Eqs. (1.1)) is chosen on the basis of agreement of the calculated and experimental [3, 4] dependence of the coordinate of a single particle on time x(t) during its acceleration behind the shock front. The line in Fig.1 shows the results of calculation of the trajectory of a single particle with $\zeta = 0.38$, while the circles show experimental results for particles of bronze with $\rho_{22} = 8.6\cdot10^3$ kg/m^3 and d = 180 ± 10 μm. The Mach number of the shock wave $M_0 = 2.6$, and the initial pressure $p^0 = 1$ atm. It follows from Fig. 1 that the formula chosen for C_d adequately describes the motion of a single particle within broad ranges of M_{12} and Re.

2. System (1.2) was solved numerically on a computer using an algorithm that consists essentially of the following. A rectangular Eulerian grid is constructed in the plane (r, z). The mesh size of the grid in terms of r and z is $2h_r$ and $2h_z$, respectively. The equations for the gas are written on the Eulerian grid with the use of an explicit finite-difference scheme

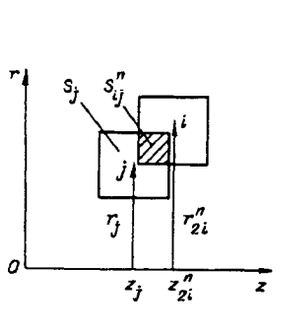

Fig 2

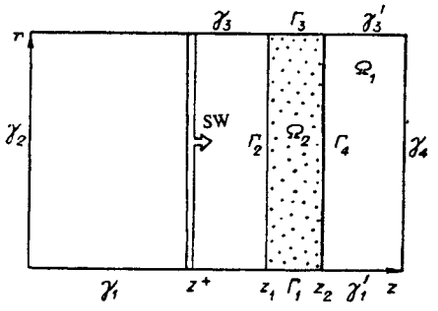

Fig. 3

of third-order accuracy (vector notation is employed also – see Eqs. (1.2)) [5, 6]. The non-collisional kinetic equation is solvedin Lagrangian variables. We choose an individual volume within the phase space of the particles $\mathcal{V}^o(t)$. The condition of conservation of the total number of particles N in the volume has the form

$$N = \int_{\mathcal{V}^o(t)} f dV \, \delta V dr_s = \text{const} \tag{2.1}$$

where $\mathcal{V}^o(t)$ is comprised of the same particles whose trajectories are determined from the equations

$$\frac{dz}{dt} = v_2, \frac{dr}{dt} = w_2, \frac{dv_2}{dt} = a_z, \frac{dw_2}{dt} = a_r, \frac{dr_s}{dt} = 0. \tag{2.2}$$

System (2.2) is consistent with the characteristics of the kinetic equation (the first equation in Eqs. (1.2)). The last equation in Eqs. (2.2) reflects the absence of particle fragmentation and coalescence. Differentiating Eq. (2.1) with respect to time and allowing for the Ostrogradskii–Gauss theorem and system (2.2), we easily obtain the non-collisional kinetic equation in Eqs. (1.2).

The region occupied by the particles is broken up at the moment t = 0 into rectangular Lagrangian cells of the size $2h_z$, $2h_r$, so that all particles within each i-th cell have the same velocity v_{2i}^0, w_{2i}^0 and radius r_i. As a result, the distribution function in the i-th particle cell at t = 0 is written as

$$f_i^0 = \frac{N_i}{V_i^0}\delta(v_2 - v_{2i}^0)\delta(w_2 - w_{2i}^0)\delta(r - r_i), \; V_i^0 = 4(r_i^0)^k h_z h_r$$

(N_i is the number of particles in the i-th cell and δ is the delta function). The individual volume $\mathcal{V}^o(t)$ will coincide with the volume of the moving cell, so the number of particles in the i-th cell remains constant. Thus, the distribution function in the i-th cell at the moment t^n will be given by the formula

$$f_i^n = \frac{N_i}{V_i^n}\delta(v_2 - v_{2i}^n)\delta(w_2 - w_{2i}^n)\delta(r - r_i), \tag{2.3}$$

where

$$V_i^n = 4(r_{2i}^n)^k h_z h_r,$$
$$v_{2i}^n = v_{2i}^{n-1} + \tau a_{zi}^{n-1}, \; w_{2i}^n = w_{2i}^{n-1} + \tau a_{ri}^{n-1},$$
$$z_{2i}^n = z_{2i}^{n-1} + \tau v_{2i}^{n-1} + a_{zi}^{n-1}\tau^2/2,$$
$$r_{2i}^n = r_{2i}^{n-1} + \tau w_{2i}^{n-1} + a_{ri}^{n-1}\tau^2/2,$$

$\tau = t^n - t^{n-1}$ is the time step. As follows from Eq. (2.3), the Lagrangian particle cells move relative of the Eulerian grid with the velocities v_{2i}^n, w_{2i}^n. The distribution function of f_j^n in the j-th Eulerian cell (EC) has the form

$$f_j^n = \sum_i^m \frac{\delta_i^n N_i}{V_i^n}\delta(v_2 - v_{2i}^n)\delta(w_2 - w_{2i}^n)\delta(r - r_i), \tag{2.4}$$

$$\delta_i^n = \frac{V_{ij}^n}{V_j}, \; V_{ij}^n = (r_{2i}^n)^k S_{ij}^n, \; V_j = (r_j)^k S_j, \; S_j = 4h_z h_r,$$

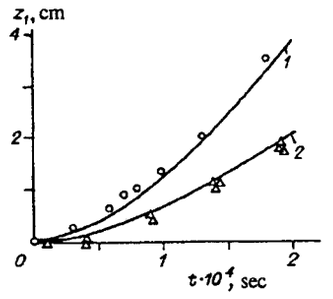

Fig. 4

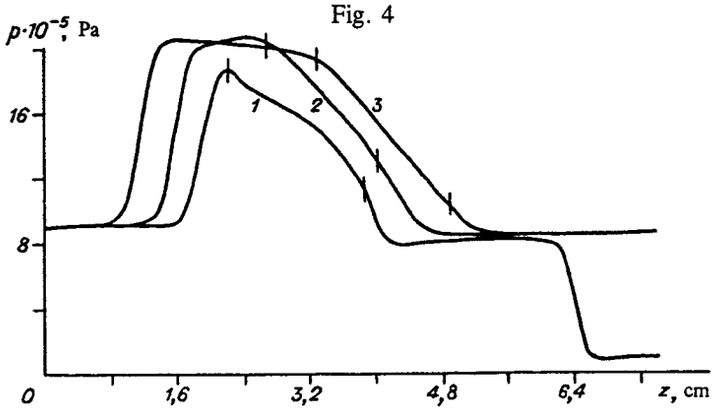

Fig. 5

where δ_i^n is the fraction of the volume occupied by the i-th particle cell in the j-th Eulerian cell; the quantities S_j and S_{ij}^n are shown in Fig. 2 for the i-th particle cell intersecting the j-th Eulerian cell. Summation in Eqs. (2.4) is performed over m particle cells intersecting the j-th Eulerian cell. We use (2.4) to find the mean value

$$\langle Q \rangle = \frac{1}{n} \int_{-\infty}^{\infty} \int_{0}^{\infty} Q f dV_\sigma dr. \tag{2.5}$$

Inserting Eqs. (2.4) into Eq. (2.5), in the j-th Eulerian cell we obtain

$$\langle Q \rangle_j^n = \left(\sum_i^m Q_i^n \delta_i^n N_i / V_i^n \right) / \left(\sum_i^m \delta_i^n N_i / V_i^n \right). \tag{2.6}$$

Formula (2.6) makes it possible to find the mean parameters of the particles in an arbitrary EC. The parameters of the gas in the particle cells were found by linear interpolation.

3. We will examine a cloud of solid spherical particles in a plane channel struck on the left side by a shock wave (Fig. 3). The cloud is uniform at the moment t = 0 and covers the entire cross section of the channel. Along z, the cloud is bounded by Γ_2 and Γ_3. The coordinates of the left and right boundaries of the cloud are z_1 and z_2. We need to calculate the pattern of flow which arises due to interaction of the shock wave with the cloud of particles. We also need to find the dependence of the coordinate of the left boundary of the cloud z_1 on time t. (The interaction of a shock wave with a cloud of particles was studied experimentally in [3, 4] and the time dependence of the left boundary of the cloud was measured). There are no particles in region Ω_1, so the parameters of the gas were found by solving the system of Eulerian equations (ideal gas) by a method of third-order accuracy. System (1.2) was solved in the region Ω_2 by the numerical method described in Part 2. In Eqs. (1.2), we put k = 0 (plane case), $\zeta = 0.38$, and D = Ḋ = 0 (laboratory coordinate system). The initial conditions were assigned in the form

$$\begin{gathered}
\rho_{11} = \rho_{11}^0,\ p = p^0,\ v_1 = w_1 = 0,\ z > z^+, \\
\rho_{11} = \rho_{11}^0 M_0^2/(1 - h + hM_0^2),\ p = p^0((1 + h)M_0^2 - h), \\
v_1 = (1 - h)c_0(M_0 - 1/M_0),\ h = (\gamma - 1)/(\gamma + 1), \\
w_1 = 0,\ M_0 = D_0/c_0,\ z < z^+, \\
m_2 = m_2^0,\ f^0 = R(r)\delta(w_2)\delta(v_2) \text{ in } \Omega_2,
\end{gathered} \tag{3.1}$$

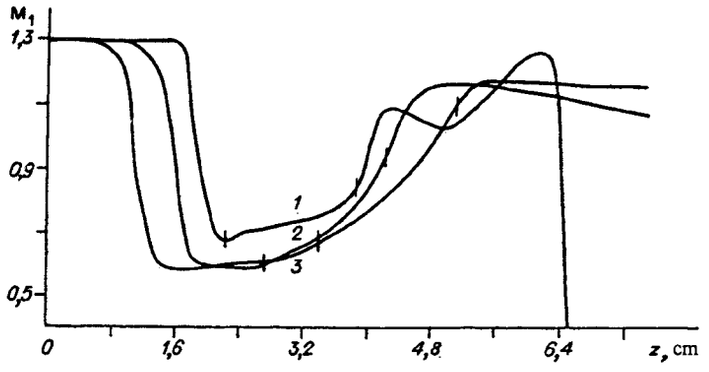

Fig. 6

where $R(r) = 6m_2^0/\pi d^3 \cdot \delta(r - d_s/2)$ for a monodisperse cloud of particles with the diameter $d = d_s$; the function R(r) for the polydisperse case will be shown below. We take $w_1 = 0$ as the boundary conditions for the gas on $\gamma_1\Gamma_1\gamma'_1\gamma_3\Gamma_3\gamma'_3$ and we assign the condition of symmetry on γ_2, γ_4 (see Fig. 3). The condition of mirror reflection is assigned for the particles on $\gamma_1\Gamma_1\gamma'_1$ and $\gamma_3\Gamma_3\gamma'_3$, while the condition of particle absorption is assigned on γ_2, γ_4. The value chosen for the parameters of the gas and the particles in the calculations were the same as in the experiments in [3, 4]. The gas was in a quiescent state ahead of the shock front: $w_1^0 = v_1^0 = 0$, $\rho_{11}^0 = 1.2$ kg/m^3, $p^0 = 10^5$ Pa, $\gamma = 1.4$ and $M_0 = 2.8$. The spherical particles examined were made of organic glass and bronze. Calculations were performed when $m_2^0 = 10^{-3}$ and $3\cdot10^{-2}$ for glass particles with $\rho_{22} = 1.2\cdot10^3$ kg/m^3 and $d_s = 300$ μm, while the coordinates of the boundaries of the cloud at $t = 0$ were $z_1 = 2\cdot10^{-2}$ m, $z_2 = 3.8\cdot10^{-2}$ m. For particles of bronze with $\rho_{22} = 8.6\cdot10^3$ kg/m^3, $d_s = 130$ μm, $m_2^0 = 10^{-3}$ and 10^{-2}, $z_1 = 1.4\cdot10^{-2}$ m, $z_2 = 2.3\cdot10^{-2}$ m.

Particle dimensions in the experiment changed within the ranged $d \sim$ 80-130 μm in the case of bronze and $d \sim$ 80-300 μm in the case of glass. The effect of polydispersity is examined below using bronze particles as an example. Our calculations showed that the presence of a small fraction does not significantly alter the pattern of gas flow or the dependence of the coordinate of the left boundary of the cloud on time.

Figure 4 shows the trajectory of the left boundary of the cloud $z_1(t)$ after interaction of the shock wave with a cloud of organic-glass particles. The circles represent experimental results from [3, 4] with a low-density cloud ($m_2^0 = 10^{-3}$), the triangles showing the data for a denser cloud ($m_2^0 = 3\cdot10^{-2}$). The results of calculations performed with $m_2^0 = 10^{-2}$ and $3\cdot10^{-2}$ are shown by curves 1 and 2, respectively. It is evident that the agreement between the experimental and theoretical results is good. For a cloud with $m_2^0 = 3\cdot10^{-2}$, Figs. 5 and 6 show the functions for pressure p(z) and local Mach number $M_1(z)$ ($M_1 = v_1/c_1$) at the moments $t = 50$, 100, and 150 μsec (curves 1-3). The vertical segments on p(z) and $M_1(z)$ represent the left and right boundaries of the cloud. It is evident that a reflected collective shock wave is formed ahead of the cloud, this wave gradually "running away" from the latter. A rarefaction wave is formed inside the cloud. The gas is accelerated inside this wave and the flow becomes supersonic near the right boundary. The rarefaction wave does not decay significantly over time and has dimensions commensurate with the dimensions of the cloud. The amplitude of the transmitted shock wave decreases relative to that of the incident wave, since the energy of the gas goes into acceleration of the cloud. The formation of the reflected shock wave is connected with slowing of the gas by the particles of the cloud. Thus, the time of formation t^* should be on the order of the time of velocity relaxation of the gas τ_v. We can evaluate τ_v from the equations of motion of the gas

$$\frac{dv_1}{dt} = -\frac{1}{\rho_{11}}\frac{\partial p}{\partial z} - \frac{3}{4}C_d\frac{m_2}{m_1}|v_1 - v_2|(v_1 - v_2)/d. \tag{3.2}$$

At the stage of formation of the collective shock wave, particle velocity v_2 is considerably lower than the velocity of the gas v_1 ($v_2 << v_1$). the second term in the right side of Eq. (3.2) can therefore be represented in the form $-v_1/\tau_v$, where

$$\tau_v = \frac{4}{3}\frac{m_1}{C_d m_2}\frac{d}{v_1}. \tag{3.3}$$

Inserting $d = 300$ μm, $C_d \sim$ 1-0.5, $m_2 = 3\cdot10^{-2}$, and $v_1 \simeq 7\cdot10^2$ into Eq. (3.3), we obtain $\tau_v \sim$ 20-40 μsec. This is close to $t^* \sim 50$ μsec (see Figs. 5 and 6). It is evident from Figs. 5 and 6 that gas motion in the system based on the center of mass

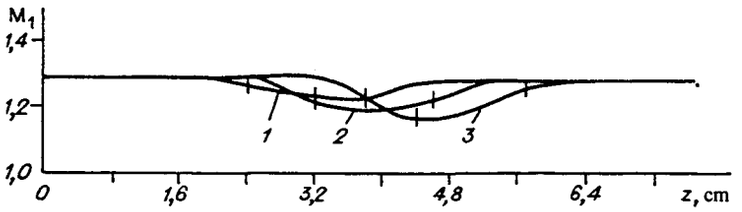

Fig. 7

of the cloud is quasisteady at t > 50 μsec. Thus, rewriting Eq. (3.2) in this system with allowance for $\partial(v_1 - v_2)/\partial t \approx 0$, $D \approx v_2$, we obtain

$$\frac{\partial p}{\partial z} \approx -\rho_{11}\dot{v}_2 - \frac{\partial}{\partial z}\rho_{11}(v_1 - v_2)^2 - \frac{3}{4}C_d\frac{m_2}{m_1}\rho_{11}|v_1 - v_2|(v_1 - v_2)/d. \tag{3.4}$$

Since the gas in the cloud and the cloud itself accelerate ($\partial/\partial z\, \rho_1(v_1 - v_2)^2 \geq 0$, $\dot{v}_2 \geq 0$, $v_1 \geq v_2$), we obtain the inequality $\partial p/\partial z \geq 0$ from Eq. (3.4). The difference $(v_1 - v_2)$ decreases with acceleration of the cloud, which leads to a corresponding reduction in the gradient $|\partial p/\partial z|$ and the amplitude of the reflected shock wave. Evident in Fig. 5 is the decrease in pressure p in the latter at t = 150 μsec compared to t = 100 μsec. The equality $\partial p/\partial z = 0$ is attained when the cloud moves at a velocity equal to the velocity of the gas $v_2 = v_1$. The reflected shock wave disappears in this case.

Figure 7 shows the relation $M_1(z)$ in the interaction of a shock wave with a cloud of particles of organic glass when the volume concentration of particles is low ($m_2^0 = 10^{-3}$). Curves 1-3 correspond to t = 50, 100, and 150 μsec. The vertical segments denote the left and right boundaries of the cloud. It is evident that flow in the cloud is supersonic ($M_1 > 1$) and that no reflected collective shock wave appears. The appearance of small perturbations ahead of the left boundary of the cloud is related to artificial viscosity.

The above analysis of gas flow makes clear the reason for the greater acceleration of a low-density cloud of particles. For such a cloud composed of organic–glass particles ($m_2^0 \approx 10^{-3}$) (see Figs. 6 and 7), gas velocity in the cloud is roughly twice as great as in a dense cloud ($m_2^0 = 3\cdot10^{-3}$) (see Figs. 5 and 6). The force f_{12} acting on a particle in the cloud is determined by the coefficient C_d and the velocity head: $f_{12} \sim C_d\rho_{11}(v_1 - v_2)^2/d$. Particle velocity $v_2 << v_1$ can be ignored in the initial stage of acceleration (t ≤ 100 μsec), so that $f_{12} \sim C_d\rho_{11}v_1^2/d$. The value of $j = \rho_{11}v_1$ is roughly the same for the high- and low-density clouds. For proof, let us examine the change in j when a stream of gas is intercepted by the front to a reflected shock wave ($m_2^0 = 3\cdot10^{-2}$). Using u to designate the velocity of the collective reflected shock wave and the superscripts − and + to denote parameters of the gas ahead of and behind the SW, we obtain the following for the flow conservation conditions

$$\rho_{11}^+(v_1^+ - u) = \rho_{11}^-(v_1^- - u),$$

from which

$$\frac{\Delta j}{\bar{j}} = \frac{\Delta\rho_{11}}{\bar{\rho}_{11}}\frac{u}{\bar{v}_1} \sim \frac{u}{v_1}, \tag{3.5}$$

where $\Delta\rho_{11} = \rho_{11}^+ - \rho_{11}^-$; $\Delta j = j^+ - j^- = \rho_{11}^+v_1^+ = \rho_{11}^-v_1^-$. Figures 5 and 6 can be used to find the velocity of the reflected shock wave $u = \Delta z/\Delta t \approx 60$ m/sec. Assuming in (3.5) that $v_1 \approx 700$ m/sec and $u \approx 60$ m/sec, we have $\Delta j/\bar{j} \sim 0.1$. The change in j with the interception of the gas by the shock wave can be ignored.

Another factor which affects f_{12} is the dependence of C_d on M_{12}. This was discussed earlier in [3, 4]. At $m_2^0 = 10^{-3}$ $M_{12} > 1$, while at $m_2^0 = 3\cdot10^{-2}$ $M_{12} < 1$. From this, with allowance for $C_d(M_{12})$, we obtain the inequality $C_d(m_2^0 = 10^{-3}) > C_d(m_2^0 = 3\cdot10^{-2})$. As our calculations showed, at t ≈ 50 μsec we have $C_d(m_2^0 = 3\cdot10^{-2}) \approx 0.44$, $C_d(m_2^0 = 10^{-3}) \approx 0.72$. Thus, ignoring the dependence of j on m_2^0 in the first approximation, we obtain the estimate

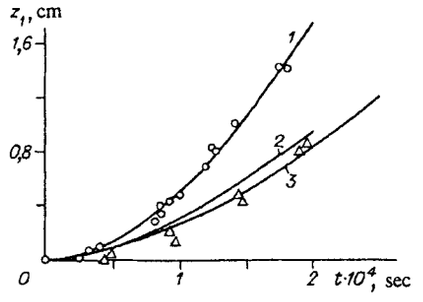

Fig. 8

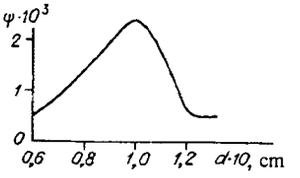

Fig. 9

$$z_1^d / z_1^p \sim f_{12}^d / f_{12}^n \sim (C_d^d v_1^d)/(C_d^n v_1^n) \sim 0.3, \qquad (3.6)$$

where the superscript d denotes a quantity evaluated with $m_2^0 = 3 \cdot 10^{-2}$ and the superscript n denotes a quantity ith $m_2^0 = 10^{-3}$. The relations shown remain in force at later moments of time, when it is impossible to ignore v_2. A ing the flow of gas and organic–glass particles in the middle of the cloud for the moment t = 150 μsec, we find

$$j^d = \rho_{11}^d (v_1 - v_2)^d = 1.6 \cdot 10^3 \text{ kg/(m}^2 \cdot \text{sec)},$$

$$(v_1 - v_2)^d = 2.3 \cdot 10^2 \text{ m/sec},$$

$$C_d^d = 0.44,\ j^n = \rho_{11}^n (v_1 - v_2)^n = 1.92 \cdot 10^3 \text{ kg/(m}^2 \cdot \text{sec)},\ (v_1 - v_2)^n = 4 \cdot 10^2 \text{ m/sec},\ C_d^n \simeq 0.5,$$

from which

$$\frac{f_{12}^d}{f_{12}^n} \sim \frac{C_d^d j^d (v_1 - v_2)^n}{C_d^n j^n (v_1 - v_2)^n} \sim 0.42.$$

It should be noted that the difference seen between f_{12}^d and f_{12}^n in the case of acceleration of a cloud of bron in a shock wave (to be examined below) is connected mainly with the relation $(C_d(M_{12})$. We thus have the follow 50 μsec for bronze particles in the middle of the cloud

$$j^d = 2.46 \cdot 10^3 \text{ kg/(m}^2 \cdot \text{sec)},\ (v_1 - v_2)^d = 3.4 \cdot 10^2 \text{ m/sec},\ C_d^d = 0.45,$$
$$j^n = 2.48 \cdot 10^3 \text{ kg/(m}^2 \cdot \text{sec)},\ (v_1 - v_2)^n = 4.5 \cdot 10^2 \text{ m/sec}\ C_d^n = 0.83,$$

from which

$$f_{12}^d / f_{12}^p \sim 0.75\ C_d^d / C_d^n \sim 0.4.$$

(Figure 8 shows the relation $z_1(t)$ in the case of acceleration of a cloud of bronze particles. The circles and triangles respectively represent experimental results obtained with $m_2^0 = 10^{-3}$ and 10^{-2}. Curves 1 and 2 show the results of calculation of the acceleration of a monodisperse cloud ($d_s = 130$ μm, $M_0 = 2.8$) when $m_2^0 = 10^{-3}$ and 10^{-2}. The qualitative pattern here is the same as in Fig. 4. Curve 3 shows the calculated acceleration of polydisperse cloud with $m_2^0 = 10^{-2}$. The size distribution for his case is the same as in Fig. 9. The quantity $\psi = \pi d^3/6\ R(d)\Delta d$, is plotted off the y-axis (Fig. 9), while diameter d is plotted off the x-axis. The distribution function R(d) at t = 0 satisfies the condition

$$\int_{d_1}^{d_2} \frac{\pi d^3}{6} R(d) d(d) = m_2^0,$$

where $d_1 = 60$ μm; $d_2 = 130$ μm; $m_2^0 = 10^{-2}$. We chose seven fractions from d_1 to d_2, with the increment $\Delta d = 10$ μm (Fig. 9). It follows from the calculations that polydispersity affects the pattern of flow in the cloud. The decrease seen in $z_1(t)$ compared to the monodisperse case $d_s = 130$ μm is connected with more rapid formation of the reflected shock wave. As was

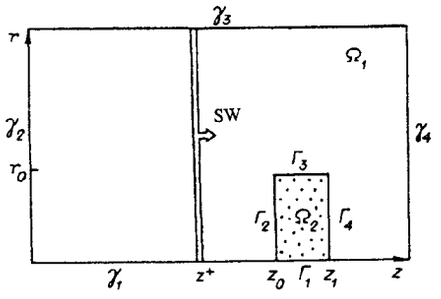

Fig. 10

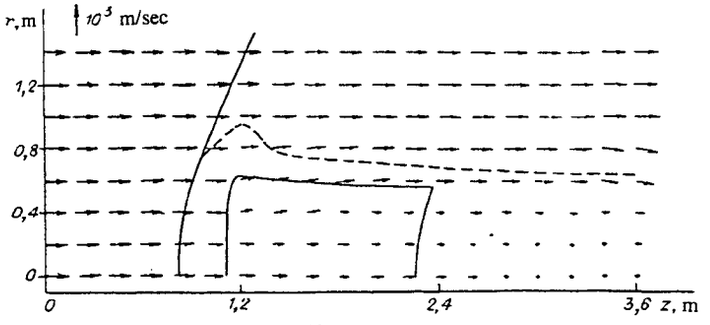

Fig. 11

noted above, $t^* \sim \tau_v \sim d$. Thus, the presence of a fine fraction reduces the time of formation of the reflected shock t^*. Another feature of flow polydispersity is the "separation" of the particles, with coarse and fine particles tending to accumulate near the left z_1 and right z_2 boundaries, respectively.

4. Let us examine a uniform cloud of spherical particles having finite dimensions with respect to z and r. A shock wave strickes the cloud from the left (Fig. 10). The symbol r_0 denotes the coordinate of the upper boundary of the cloud at the initial moment $t = 0$. The remaining notation coincides with the notation used in Fig. 3. It is assumed that the cloud is axisymmetric and is in an infinite region filled with gas. (In the numerical calculations, the region Ω_1 is bounded by γ_2, γ_3, and γ_4, for which mirror symmetry was specified; on γ_1, we set $w_1 = 0$.) The equations of an ideal gas were solved in Ω_1, while system (1.2) was solved in Ω_2. Here, we set $\zeta = 0.25$, $k = 1$ (axisymmetric case). The calculations were performed in the system based on the center of mass of the cloud. The initial conditions were given by Eqs. (3.1) with the following parameters for gas and particles: $\rho_{11}^0 = 1$ kg/m^3, $p^0 = 8.64 \cdot 10^4$ Pa, $\gamma = 1.4$, $M_0 = 3$, $z_0 = 0.9$ m, $z_1 = 1.9$ m, $r_0 = 0.6$ m, $\rho_{22} = 2.7 \cdot 10^3$, $d_s = 4 \cdot 10^{-3}$ m, $m_2^0 = 2 \cdot 10^{-2}$ (z_0 and z_1 are the coordinates of the boundaries of the cloud with respect to z; r_0 is the radius of the cloud) (Fig. 10). The boundary conditions for the gas were describe above. For the particles, we assumed that mirror reflection occurred on the axis $r = 0$ and particle absorption took place on γ_2, γ_3, γ_4. Reflected and transmitted shock waves resulted from the interaction of the incident shock with the cloud. The transmitted wave left the theoretical region through the boundary γ_4, while the reflected wave appeared in front of the cloud.

The arrows in Fig. 11 show the velocity field of the gas at $t = 5.68 \cdot 10^{-3}$ sec. The solid line show the reflected shock wave and the boundary of the cloud. The dashed line shows the Mach line ($M = 1$). It is evident that a stagnant region in which gas velocity is considerably lower than in the external region ($r > 0.6$ m) develops behind the cloud. A constant negative pressure gradient is established inside the cloud along z. This gradient offsets the force F_{12}^z which acts on the gas from the direction of the particles. Figure 12 shows the relation p(z) at $t = 5.68 \cdot 10^{-3}$ sec in three sections $r = \text{const}$. Line 1 corresponds to the axis $r = 0$, 2 corresponds to the boundary of the cloud $r = 0.6$ m, and 3 corresponds to $r = 1$ m. An increase in r leads to a decrease in the amplitude of the shock wave and the pressure gradient in the cloud, as well as to displacement of the front downstream.

Figure 13 shows the field of particle velocity in the cloud at $t = 5.68 \cdot 10^{-3}$ sec. It follows from the figure that the cloud is compressed along the z axis over time and particles are carried into the external region ($r > 0.6$ m) through the upper boundary Γ_3. Appreciably greater deformation of the cloud occurs when the cloud interacts with a shock wave with $M_0 = 10$. Figure 14 shows the position of the centers of particle cells at $t = 2.9 \cdot 10^{-2}$ sec as a result of the interaction of a shock wave ($M_0 = 10$) with a cloud of particles having the following dimensions at $t = 0$: $z_0 = 6$ m, $z_1 = 13.5$ m, $r_0 = 2.75$ m, m_2^0

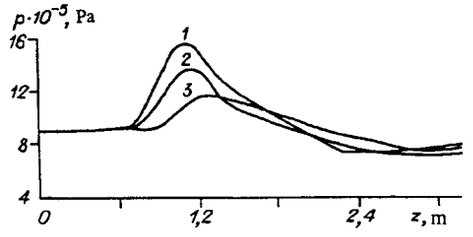

Fig. 12

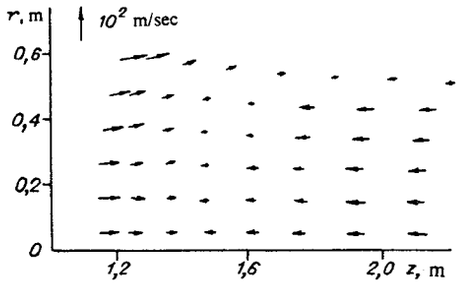

Fig. 13

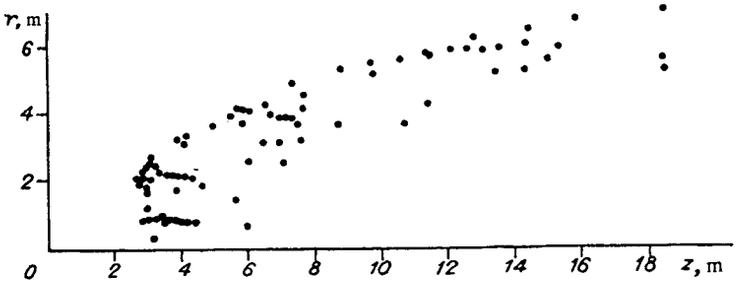

Fig. 14

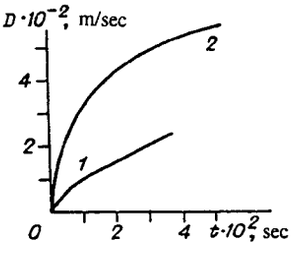

Fig. 15

$= 2 \cdot 10^{-2}$. The deformation of the cloud in the internal region ($r \lesssim 2.8$ m) results in the formation of a dense core ($m_2 \sim 4 \cdot 10^{-2}$). Particles leave this core on the windward side and form a low-density ($m_2 \sim 10^{-4}$-10^{-3}) "tail" that extends downstream. The appearance of the tail is connected with the fact that gas velocity and the coefficient C_d are greater in the external region ($r \gtrsim 2.8$ m) than in the internal region ($r \lesssim 2.8$ m). Thus, the force $f_{12} \sim C_d j(v_1 - v_2)$ acting on each particle in the external region will also be greater than the corresponding force in the internal region.

The collective effects described above have a significant influence on the acceleration of the center of mass of the cloud. Figure 15 shows the dependence of the velocity of the center of mass D on time t for $m_2^0 = 2 \cdot 10^{-2}$ and $5 \cdot 10^{-4}$ (lines 1 and 2) after the interaction of a cloud of finite dimensions ($z_0 = 0.9$ m, $z_1 = 1.9$ m, $r_0 = 0.6$ m) with a shock wave with $M_0 = 3$. Velocity D for the denser cloud ($m_2^0 = 2 \cdot 10^{-2}$) is half that for the less dense cloud ($m_2^0 = 5 \cdot 10^{-4}$). This effect is connected with a difference in the character of flow around the cloud in each of the two cases. The flow in the low-density cloud is supersonic ($M_{12} > 1$), while flow in the high-density cloud is subsonic ($M_{12} < 1$). As a result, the force $f_{12} \sim C_d(M_{12}) j(v_1 - v_2)/2$ acting on a particle in the low-density cloud will be greater than the corresponding force acting on a particle in the high-density cloud.

In conclusion, we thank V. M. Boiko for discussing the results of the study with us.

REFERENCES

1. S. P. Kiselev and V. M. Fomin, "Continuum-discrete model for a mixture of a gas and solid particles with a low volume concentration of particles," Prikl. Tekh. Fiz., No. 2 (1986).

2. S. P. Kiselev, G. A. Ruev, A. P. Trunev, et al., Shock-Wave Processes in Two-Component and Two-Phase Media [in Russian], Nauka, Novosibirsk (1992).
3. V. M. Boiko, Investigation of the Dynamics of the Acceleration, Destruction, and Ignition of Particles Behind Shock Waves by the Method of Laser Visualization: Author's Abstract of Physico-Mathematical Sciences Candidate Dissertation, Novosibirsk (1984).
4. V. M. Boiko, A. V. Fedorov, V. M. Fomin, et al., "Ingition of small particles behind shock waves," in Shock Waves, Explosions, and Detonations, Progress in Astronautics and Aeronautics, Vol. 87 New York (1983).
5. V. V. Rusanov, "Third-order difference scheme for the through calculation of discontinuous solutions," Dokl. Akad. Nauk SSSR, **180**, No. 6 (1968).
6. N. P. Gridnev, S. S. Katsnel'son, and V. P. Fomichev, Nonuniform MHD-Flows with a T-Layer [in Russian], Nauka, Novosibirsk (1984).